Processing and Application of Ceramics 11 [2] (2017) 120–126
https://doi.org/10.2298/PAC1702120C

First-principles studies on band structure and mechanical properties of $BiFeO_3$ ceramics under high pressure

Ramanathan Chandiramouli*, Veerappan Nagarajan

School of Electrical & Electronics Engineering SASTRA University, Tirumalaisamudram, Thanjavur 613 401, India

Received 31 January 2017; Received in revised form 18 April 2017; Accepted 11 May 2017

Abstract

Mechanical properties and band structure of rhombohedral $BiFeO_3$ nanostructures were studied using density functional theory for different pressures in the range from 0 to 50 GPa. The elastic constant of $BiFeO_3$ nanoceramics was determined and different moduli were calculated for various applied pressures. The bulk (B) and shear (G) modulus show an increasing trend on applied high pressure. The findings of the present work also confirm that the hardness of $BiFeO_3$ increases with the applied pressure. The ductility of $BiFeO_3$ nanostructure increases upon increasing the pressure, which is confirmed from Poisson's ratio and B/G ratio. The band structure studies were also carried out under high pressure and showed that the band gap decreases upon increase in the applied pressure.

Keywords: *$BiFeO_3$, nanostructure, first-principles studies, band gap, ductility, Poisson's ratio, elastic constant*

I. Introduction

Nowadays, research community focuses on multiferroics, a class of materials with multifunctional physical properties. Moreover, materials in the class of single phase multiferroics (such as $BiFeO_3$) display both ferroelectric and ferromagnetic characteristics in the same phase, which enables them promising applications. Thus, they can be used in spintronic devices, where ferroelectricity can be controlled using a magnetic field or magnetism can be manipulated by applied electric field. Among multiferroics, bismuth ferrite is of special interest, since it exhibits attractive magnetoelectric properties at room temperature and is ferroelectric below Curie temperature, T_c = 820–850 °C and antiferromagnetic below Neel temperature, T_N = 370–380 °C with G-type antiferromagnetic ordering [1,2]. Besides, $BiFeO_3$ materials show modified properties with the substitution of Bi^{3+} and Fe^{3+} with La^{3+} and Mn^{3+}, respectively [3]. Dhanalakshmi *et al.* [4] have studied the influence of Mn doping on structure and dielectric properties of $BiFeO_3$ nanoceramics. Neaton *et al.* [5] studied the polarization in $BiFeO_3$ using local spin density and estimated the band gap as 1.9 eV. Moreover, from the experimental reports it is known that the band gap of $BiFeO_3$ varies between 1.9–2.8 eV at ambient temperature [6–8]. Antonov *et al.* [9] used first-principles study to investigate the effect of La^{3+} and Mn^{3+} substitution on structure and properties of multiferroic $BiFeO_3$. Hussain *et al.* [10] reported about chemical pressure red shift in energy band gap in Sr doped $BiFeO_3$. Dai *et al.* [11] investigated the stoichiometric (0001) polar surface multiferroic $BiFeO_3$ nanostructures and reported that spontaneous polarization and weak ferromagnetism showed enhanced character due to the relaxation and rehydration of surface atoms. Xue *et al.* [12] studied microstructure, ferroelectric, magnetic and optical properties on Nd doped $BiFeO_3$ thin films, whereas Durga Rao *et al.* [13] studied the structural, magnetic and electrical properties of Ho substituted $BiFeO_3$ polycrystalline compounds. From the previous reports it is evident that by doping or by imposing pressure on $BiFeO_3$, the structural and electronic properties can be changed. The density functional theory is an efficient method to investigate the structural stability, electronic and mechanical properties of $BiFeO_3$ nanostructures upon applying pressure. However, from the previously reported literature it is inferred that there are only few reports based on studying the structural and electronic properties of

*Corresponding author: tel: +91 9489 566466,
fax: +91 4362 264120, e-mail: *rcmoulii@gmail.com*

$BiFeO_3$ nanostructures on various applied pressure [14]. This motivated us to carry out the present work, in which mechanical and electronic properties of $BiFeO_3$ are studied under pressure and the results are reported.

II. Computational details

The calculation in the present work was carried out with the generalized gradient approximation (GGA) in combination with Perdew-Burke-Ernzerhoff (PBE) scheme [15–17]. The elastic constants and mechanical properties of BiFeO3 were obtained based on the density functional theory (DFT) method. The SIESTA code was used in the present work for the optimization of $BiFeO_3$ nanostructures [18]. The generalized gradient approximation (GGA) of Perdew-Burke-Ernzerhoff (PBE) scheme was used to estimate the exchange-correlation energy of $BiFeO_3$ nanostructures. The plane-wave basis set with the energy cut-off of 400 eV was used during the calculation of $BiFeO_3$ nanostructures. A vacuum slab of 15 Å was selected during calculation. The energy integration in the first irreducible Brillouin zone was selected as 10 × 10 × 8 Monkhorst-Pack k-point meshes [19]. The self-consistent convergence of the total energy was obtained in the order of 10^{-6} eV/atom. The wave function of bismuth, iron and oxygen atoms were expanded in terms of double zeta polarization (DZP) [20,21] basis set, which mainly depends on the numerical orbitals. The electro-static interaction between the valence electrons and ionic core was represented in terms of ultra-soft pseudo-potentials.

III. Results and discussion

3.1. Structure of $BiFeO_3$ ceramics

The structure of $BiFeO_3$ is a highly distorted rhombohedral perovskite with space group of *R3c* [22]. When compared to cubic $Pm\bar{3}m$ structure the rhombohedral structure is observed with an anti-phase tilt of the nearest FeO_6 octahedra and a displacement of the Bi^{3+} and Fe^{3+} cations from their centro-symmetric positions along (111) plane. Moreover, the theoretical first-principles calculations have found a single pressure-induced phase transition from the rhombohedral *R3c* structure to an orthorhombic *Pnma* structure at 13 GPa [23]. Finally, the theoretical [24] and experimental studies [25,26] show the occurrence of electric and magnetic phase transitions above 50 GPa in $BiFeO_3$, but no phase transition below 50 GPa.

In the present work, the elastic properties of G-type rhombohedral antiferromagnetic (AFM) structure with space group *R3c* was used to study the influence of pressure acting on $BiFeO_3$ nanostructures. The generalized gradient approximation (GGA) was used to calculate elastic constants rather than local density approximation (LDA), since the structural properties can be calculated more efficiently by GGA than LDA, which is one of the crucial importance in calculating the elastic constants.

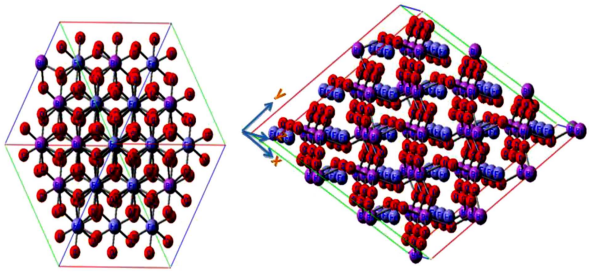

Figure 1. Schematic diagram of $BiFeO_3$ nanostructures with periodic boundary condition

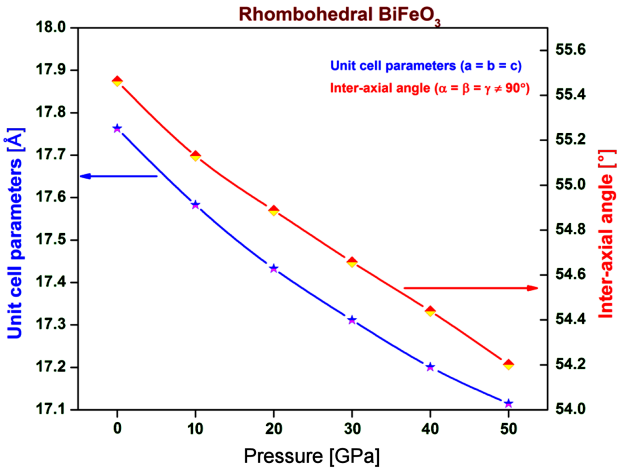

Figure 2. Variation in unit cell parameters and inter-axial angle for various applied pressures

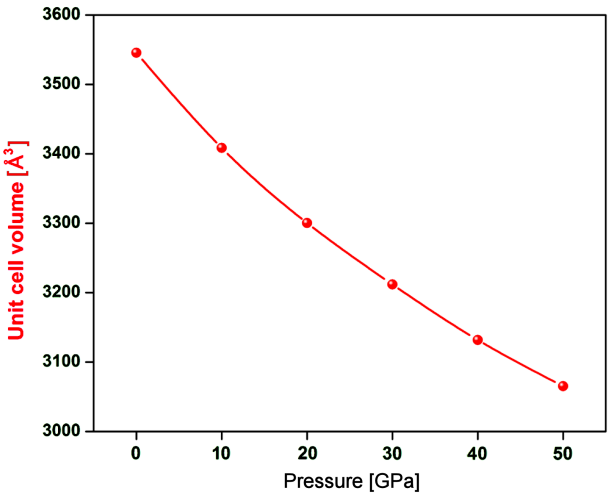

Figure 3. Variation of unit cell volume for various pressures

Figure 1 represents the schematic diagram of $BiFeO_3$ nanostructures with periodic boundary condition.

Before studying the pressure-induced electronic and mechanical properties of rhombohedral $BiFeO_3$ in detail, we first studied the pressure-dependence of the rhombohedral unit cell parameters and volume, which gives valuable inference. Figures 2 and 3 refer to the pressure-dependence of unit cell parameter and unit cell volume of rhombohedral $BiFeO_3$ nanostructure, respec-

tively. It is clearly observed that the volume shrinks and unit cell parameters, such as lattice constant and interaxial angle, decrease owing to increase in the external pressure applied on $BiFeO_3$ nanostructure from 0 to 50 GPa. The result of the present study is in good agreement with the reported experimental work [27]. Moreover, the geometrical parameters of $BiFeO_3$ vary with pressure, but the rhombohedral structure is retained even at high pressure (50 GPa) without any phase transition as validated by experiments [25].

3.2. Mechanical properties under high pressure

In order to study the mechanical properties of $BiFeO_3$ nanoceramics, the elastic constant was calculated. It is well known that rhombohedral crystal structure have six independent elastic constants namely, C_{11}, C_{12}, C_{13}, C_{14}, C_{33} and C_{44} [14,28]. The mechanical stability requires the following limitations for the elastic constants:

$$C_{33} > 0 \tag{1}$$

$$C_{44} > 0 \tag{2}$$

$$C_{11} - |C_{12}| > 0 \tag{3}$$

$$(C_{11} + C_{12}) \cdot C_{33} - 2C_{13}^2 > 0 \tag{4}$$

$$(C_{11} - C_{12}) \cdot C_{44} - 2C_{14}^2 > 0 \tag{5}$$

Table 1 presents calculated elastic constants of $BiFeO_3$ nanostructures under high pressure. Besides, the elastic constants of rhombohedral $BiFeO_3$ nanostructures are found to satisfy the above condition, which confirms the mechanical stability criteria.

In the next step we determined the Voigt bulk modulus (B_V), Reuss bulk modulus (B_R), Hill bulk modulus (B_H), Voigt shear modulus (G_V), Reuss shear modulus (G_R), Hill shear modulus (G_H), Voigt Young's modulus (Y_V), Reuss Young's modulus (Y_R) and Hill Young's modulus (Y_H), and their values are given in Table 2. It is known that for rhombohedral lattice, $_V$, G_V, B_R and G_R [28] are represented with the following equations:

$$B_V = \frac{2C_{11} + C_{33} + 2C_{12} + 4C_{13}}{9} \tag{6}$$

$$5G_V = (2C_{11} + C_{33}) - (C_{12} + 2C_{13}) + 3\left(2C_{44} + \frac{C_{11} - C_{12}}{2}\right) \tag{7}$$

$$1/B_R = (2C_{11} + C_{33}) + 2(C_{12} + 2C_{13}) \tag{8}$$

$$15/G_R = 4(2C_{11} + C_{33}) - 4(C_{12} + 2C_{13}) + 3(2C_{44} + C_{66}) \tag{9}$$

Moreover, the Hill moduli [29] are obtained by the following formulas:

$$G_H = \frac{G_R + G_V}{2} \tag{10}$$

$$B_H = \frac{B_R + B_V}{2} \tag{11}$$

Furthermore, the Young's modulus (E) and Poisson's ratio (ν) can be expressed using bulk modulus (B) and shear modulus (G) values by the following equations:

$$\nu = \frac{3B - 2G}{6B + 2G} \tag{12}$$

$$E = \frac{9B \cdot G}{3B + G} \tag{13}$$

It is evident from the elastic constants that upon increase in the pressure from 0 to 50 GPa, the magnitude of elastic constants increases almost in a linear fashion. Figure 4 illustrates the plot of pressure versus bulk modulus and shear modulus of $BiFeO_3$ nanostructures. Moreover, for all the cases namely Voigt, Reuss and Hill moduli, a linear increase in bulk and shear modulus upon increase in pressure is observed. It is well known that if bulk modulus of $BiFeO_3$ is small, then the material is less hard. However, the large value of bulk modulus gives rise to increase in the hardness [30]. Furthermore, $BiFeO_3$ exhibits an increase in the bulk modulus with the increase in the pressure. From the results, it is inferred that the application of pressure makes $BiFeO_3$ ceramics harder.

Table 1. Elastic constants of rhombohedral $BiFeO_3$ nanoceramics at various pressures

Pressure [GPa]	C_{11}	C_{12}	C_{13}	C_{14}	C_{33}	C_{44}
0	551.63	283.65	107.01	13.29	530.20	129.66
10	610.01	319.68	114.53	14.99	586.23	139.04
20	759.65	413.6	133.66	20.33	729.58	164.42
30	852.38	469.86	145.53	23.51	814.28	180.36
40	939.61	523.16	164.44	26.55	899.48	197.07
50	1046.7	588.14	188.82	29.36	1002.93	217.06

Table 2. Bulk (B), shear (G) and Young's modulus (E) of $BiFeO_3$ nanoceramics under high pressure

Pressure [GPa]	B_R [GPa]	B_V [GPa]	B_V [GPa]	G_R [GPa]	G_V [GPa]	G_V [GPa]	E_R [GPa]	E_V [GPa]	E_V [GPa]
0	286.15	292.09	289.12	143.53	154.38	148.95	397.42	397.42	502.78
10	315.54	322.63	319.09	155.23	168.48	161.86	433.54	433.54	558.01
20	391.00	401.19	396.1	185.14	204.9	195.02	523.31	523.31	699.13
30	436.66	448.99	442.83	204.07	227.6	215.84	580.71	580.71	782.24
40	484.51	498.09	491.3	222.54	248.92	235.73	633.68	633.68	862.51
50	543.53	558.66	551.1	245.22	274.72	259.97	699.67	699.67	959.31

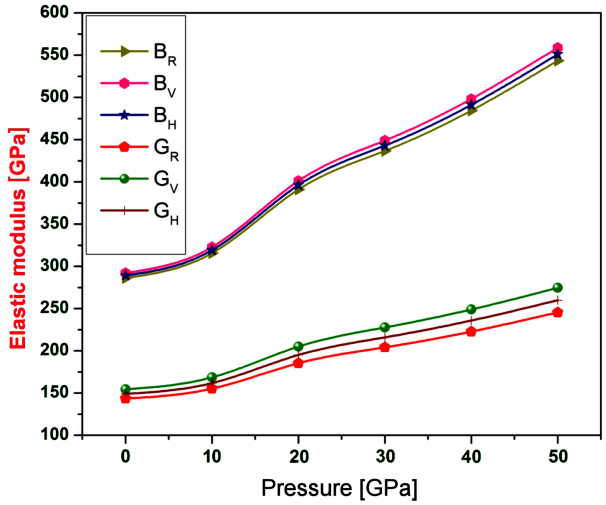

Figure 4. Plot of pressure versus bulk modulus and shear modulus

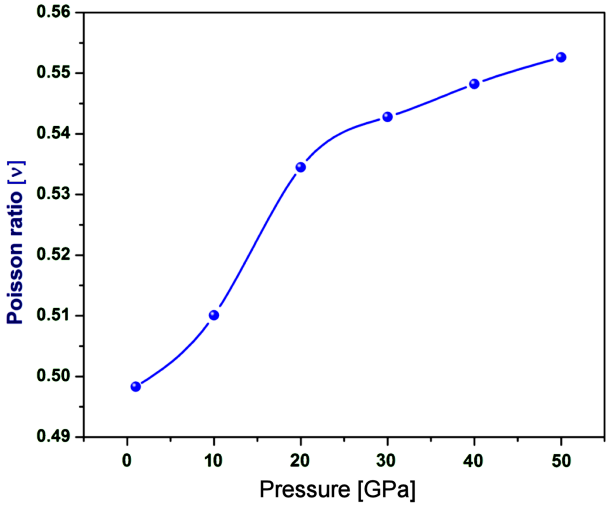

Figure 5. Poisson's ratio versus pressure of $BiFeO_3$ nanostructures

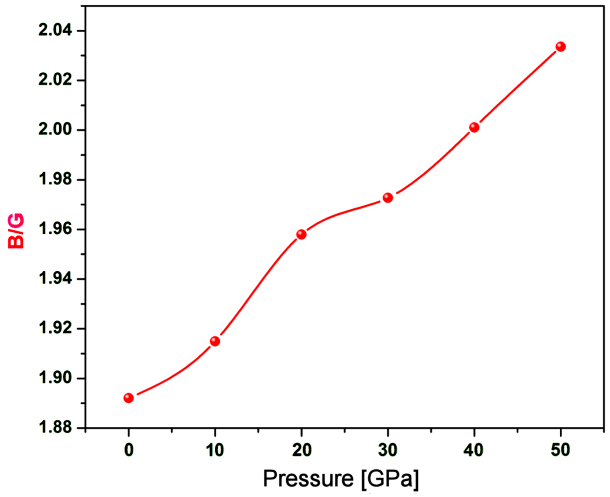

Figure 6. Pressure versus *B/G* ratio plot of $BiFeO_3$ nanostructures

However, the hardness of $BiFeO_3$ also depends on the shear modulus (G) of the nanomaterial. Moreover, the small value of G indicates that the compound is brittle in nature. Observing the results of shear modulus only for 0 GPa, the shear modulus is found to be low, whereas for high pressure applied to $BiFeO_3$ it shows increasing trend in the value of G [31]. Thus, it is clearly evident that the applied high pressure makes $BiFeO_3$ more ductile in nature. It is well known that the high degree of ductility occurs due to the metallic bonding nature observed in metals. Moreover, when the applied pressure on $BiFeO_3$ increases, the valence electrons are delocalized across the atoms in $BiFeO_3$ nanostructure. The delocalization of electrons facilitates the electrons to move easily along $BiFeO_3$ nanostructures, resulting in the ductile properties. Thus, it is observed that in $BiFeO_3$ ceramics, the applied pressure makes the material harder with the enhancement of the ductility. Furthermore, the other important parameter for studying the resistance towards uniaxial tension is observed from Young's modulus (E). The large value of E indicates the stronger tensile strength [32]. The Young's modulus of $BiFeO_3$ shows an increasing trend upon increase in the pressure up to 50 GPa. The results of E show that $BiFeO_3$ ceramics withstands the load against elongation upon increase in pressure. It is evident from the results of B, G and E values of $BiFeO_3$ ceramics that the increase in the pressure tends to increase the ductility of the material.

Poisson's ratio (ν) plays an important role in mechanical engineering design. It illustrates the negative ratio of transverse and longitudinal strains. A high value of Poisson's ratio, greater than 0.26, generally represents good ductility. In contrast a low value infers the brittle nature [33]. Figure 5 depicts the plot of Poisson's ratio versus pressure. Even at 0 GPa, the Poisson's ratio is found to be 0.496 for $BiFeO_3$ nanostructure. In addition, with applying pressure to $BiFeO_3$ nanostructure, the Poisson's ratio reaches the value of 0.554 at 50 GPa. Thus, it is confirmed that applied high pressure makes $BiFeO_3$ nanostructure to become more ductile, which is consistent with the obtained results for bulk and shear moduli. The reason behind the improved ductility of $BiFeO_3$ lies in the electrons being delocalized similar to the ductile property of metal.

Figure 6 represents the plot of pressure versus B/G ratio. The toughness of the material is analysed by the degree of plasticity/ductility of the nanomaterial. Furthermore, the ductile/brittle behaviour of the material can be ascertained by Pugh's ratio [34]. If the value of B/G ratio of compound is higher than 1.75, the material is said to be ductile [35,36]. From Fig. 6, it is clearly revealed that even at 0 GPa, $BiFeO_3$ nanostructure possesses a B/G ratio of 1.89, which confirms that $BiFeO_3$ exhibits ductile nature. Upon increasing the pressure, the B/G ratio finally reaches the value of 2.03 for the pressure of 50 GPa. B/G ratio plot shows that under high pressure $BiFeO_3$ ceramics becomes more ductile. The

present work should be compared with the previously reported work of Shang *et al.* [14]. They studied the elastic properties of rhombohedral $BiFeO_3$ using quantum mechanical calculations. In their work elastic constants, bulk and shear moduli have almost same values, which further strengthens our results.

Figure 7 depicts universal anisotropy (A^U) for the applied pressure for $BiFeO_3$ nanostructure. It is well known that for isotropic materials $A^U = 0$. Moreover, a large value of A^U specifies larger material anisotropy. From the results of A^U, it is observed that for the pressure range from 0 to 50 GPa, the value of A^U varies from 0.4 to 0.625.

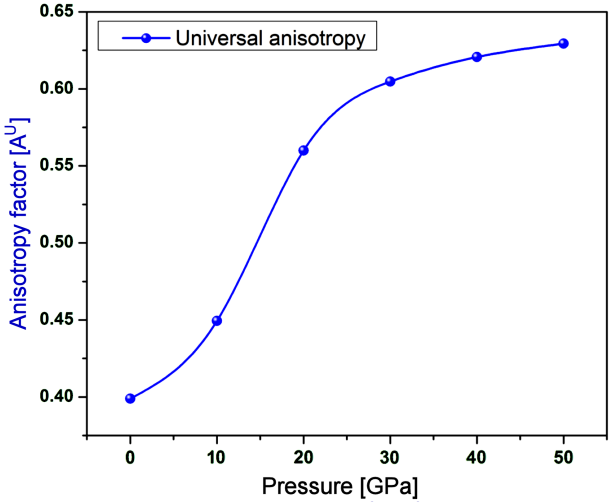

Figure 7. Pressure versus universal anisotropy of $BiFeO_3$ nanoceramics

The result shows that when the applied pressure increases, the anisotropy of $BiFeO_3$ nanostructure increases. The propagation of microcracks and lattice distortion arises in the material due to the elastic anisotropy [32]. In the present work, the applied high pressure turns $BiFeO_3$ nanoceramics to deviate from its lattice, which facilitates the ductile property of $BiFeO_3$ nanomaterial under high pressure.

3.3. Band structure studies under high pressure

The material properties of $BiFeO_3$ nanostructures can be invoked by analysing the band structure of the material [37–39]. The band gap of the material can be studied across the gap along the gamma point (Γ). Furthermore, if the channels cross the Fermi energy level (E_L), it refers the metallic nature of the material [40,41]. However, in the present study for 0 GPa pressure (Fig. 8), the band gap of $BiFeO_3$ nanostructure is estimated to be around 1.92 eV. Moreover, it is well known that since DFT method is nearer to ground state, the exchange-correlation function is taken into account for outermost electrons, which in turn underestimates the band gap.

However, the present study is carried out for $BiFeO_3$ nanoceramics for different pressures from 0 to 50 GPa in which the band gap under pressure can be relatively compared, which gives better results. On applying the pressure of 10 GPa as shown in Fig. 9, the band gap decreases due to the applied pressure.

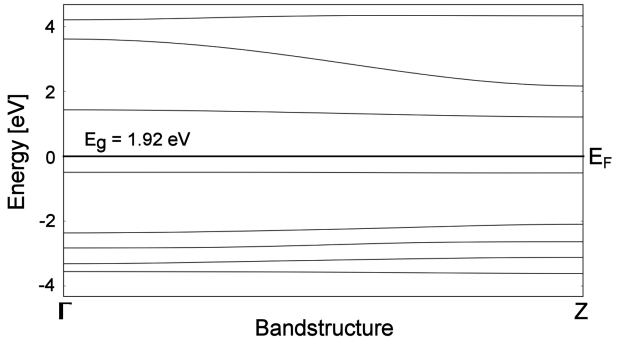

Figure 8. Band structure of $BiFeO_3$ nanostructure at 0 GPa

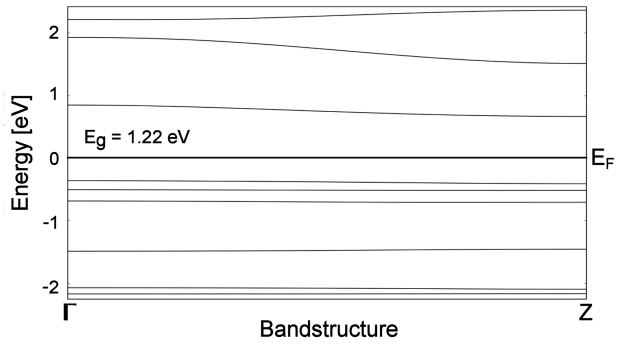

Figure 9. Band structure of $BiFeO_3$ nanostructure at 10 GPa

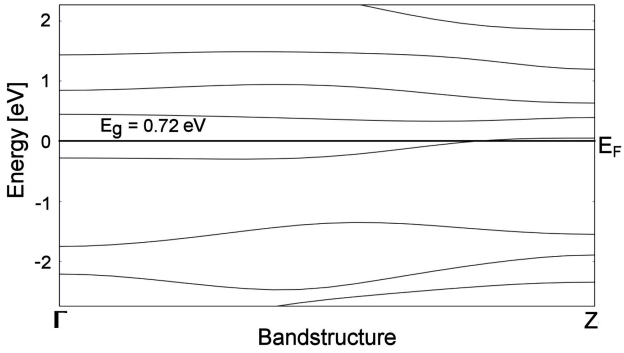

Figure 10. Band structure of $BiFeO_3$ nanostructure at 50 GPa

The decrease in the band gap is governed by the fact that the applied pressure results in lattice distortion in $BiFeO_3$ nanostructures, which in turn decreases the band gap. For the pressure of 10 GPa (Fig. 9), the band gap at Γ point decreases to 1.22 eV. In addition, on applying the pressure of 50 GPa to $BiFeO_3$ nanostructures, the band gap further decreases to 0.72 eV (Fig. 10). Figure 11 illustrates the comparative variation of band structure upon applied pressure of $BiFeO_3$ nanostructure for a pressure of 0, 10 and 50 GPa. The band structure studies show that upon increasing the pressure applied to $BiFeO_3$ nanostructure, the band gap decreases due to the lattice distortion and it turns $BiFeO_3$ nanostructure to near metallic in nature.

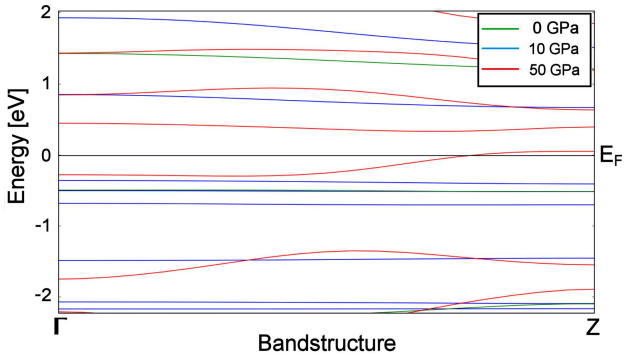

Figure 11. Comparative diagram of $BiFeO_3$ nanoceramics band structure at 0, 10 and 50 GPa

IV. Conclusions

The mechanical properties and band structure of $BiFeO_3$ nanostructures were studied using DFT method employing GGA/PBE functional. The elastic constants for rhombohedral $BiFeO_3$ nanostructures were calculated and different modulus such as bulk, shear and Young's modulus were determined. The hardness of the material increases due to the applied high pressure. Furthermore, on increasing the pressure the ductility of $BiFeO_3$ nanoceramics increases, which is confirmed from the results of Poisson's ratio and B/G ratio. Moreover, the universal anisotropy increases upon increasing the pressure. This shows that lattice distortion takes place due to the applied high pressure. The band structure also shows that upon increase in pressure, the band gap decreases. The findings of the present work confirm that $BiFeO_3$ nanoceramics become more ductile and the band structure also decreases under high pressure.

References

1. V. Kumar, S. Singh, "Improved structure stability, optical and magnetic properties of Ca and Ti co-substituted $BiFeO_3$ nanoparticles", *Appl. Surf. Sci.*, **386** (2016) 78–83.
2. W. Kaczmarek, Z. Pajak, M. Polomska, "Differential thermal analysis of phase transitions in $(Bi_{1-x}La_x)FeO_3$ solid solution", *Solid State Commun.*, **17** (1975) 807–810.
3. J.R. Sahu, C.N.R. Rao, "Beneficial modification of the properties of multiferroic $BiFeO_3$ by cation substitution", *Solid State Sci.*, **9** (2007) 950–954.
4. B. Dhanalakshmi, K. Pratap, B.P. Rao, P.S.V.S. Rao, "Effects of Mn doping on structural, dielectric and multiferroic properties of $BiFeO_3$ nanoceramics", *J. Alloys Compd.*, **676** (2016) 193–201.
5. J.B. Neaton, C. Ederer, U.V. Waghmare, N.A. Spaldin, K.M. Rabe, "First-principles study of spontaneous polarization in multiferroic $BiFeO_3$", *Phys. Rev. B - Condens. Matter Mater. Phys.*, **71** (2005) 014113.
6. A. Mukherjee, S.M. Hossain, M. Pal, S. Basu, "Effect of Y-doping on optical properties of multiferroics $BiFeO_3$ nanoparticles", *Appl. Nanosci.*, **2** (2012) 305–310.
7. S.J. Clark, J. Robertson, "Band gap and Schottky barrier heights of multiferroic $BiFeO_3$", *Appl. Phys. Lett.*, **90** (2007) 132903.
8. T.P. Gujar, V.R. Shinde, C.D. Lokhande, "Nanocrystalline and highly resistive bismuth ferric oxide thin films by a simple chemical method", *Mater. Chem. Phys.*, **103** (2007) 142–146.
9. V. Antonov, I. Georgieva, N. Trendafilova, D. Kovacheva, K. Krezhov, "First principles study of structure and properties of La- and Mn-modified $BiFeO_3$", *Solid State Sci.*, **14** (2012) 782–788.
10. S. Hussain, S.K. Hasanain, "Chemical pressure induced red shift in band gap and d-d transition energies in Sr doped $BiFeO_3$", *J. Alloys Compd.*, **688** (2016) 1151–1156.
11. J.Q. Dai, J.W. Xu, J.H. Zhu, "First-principles study on the multiferroic $BiFeO_3$ (0001) polar surfaces", *Appl. Surf. Sci.*, **392** (2017) 135–143.
12. X. Xue, G. Tan, W. Liu, H. Hao, "Study on pure and Nd-doped $BiFeO_3$ thin films prepared by chemical solution deposition method", *J. Alloys Compd.*, **604** (2014) 57–65.
13. T. Durga Rao, T. Karthik, A. Srinivas, S. Asthana, "Study of structural, magnetic and electrical properties on Ho-substituted $BiFeO_3$", *Solid State Commun.*, **152** (2012) 2071–2077.
14. S.L. Shang, G. Sheng, Y. Wang, L.Q. Chen, Z.K. Liu, "Elastic properties of cubic and rhombohedral $BiFeO_3$ from first-principles calculations", *Phys. Rev. B - Condens. Matter Mater. Phys.*, **80** (2009) 052102.
15. J. Perdew, K. Burke, Y. Wang, "Generalized gradient approximation for the exchange-correlation hole of a many-electron system", *Phys. Rev. B.*, **54** (1996) 16533–16539.
16. J. Perdew, J. Chevary, S. Vosko, K. Jackson, M. Pederson, D. Singh, C. Fiolhais, "Atoms, molecules, solids, and surfaces: Applications of the generalized gradient approximation for exchange and correlation", *Phys. Rev. B.*, **46** (1992) 6671–6687.
17. J.P. Perdew, K. Burke, M. Ernzerhof, "Generalized gradient approximation made simple", *Phys. Rev. Lett.*, **77** (1996) 3865–3868.
18. J.M. Soler, E. Artacho, J.D. Gale, A. Garcia, J. Junquera, P. Ordejon, D. Sanchez-Portal, "The SIESTA method for ab initio order-N materials simulation", *J. Physics Condens. Matter* ., **14** (2002) 2745–2779.
19. H.J. Monkhorst, J.D. Pack, "Special points for Brillouin-zone integrations", *Phys. Rev. B.*, **13** (1977) 5188–5192.
20. G. Dhivya, V. Nagarajan, R. Chandiramouli, "First-principles studies on switching properties of azobenzene based molecular device", *Chem. Phys. Lett.*, **660** (2016) 27–32.
21. M. Deekshitha, A. Srivastava, R. Chandiramouli, "Investigation on transport property of In_2O_3 molecular device - A first-principles study", *Microelectron. Eng.*, **151** (2016) 1–6.
22. P. Fischer, M. Polomska, I. Sosnowska, M. Szymanski, "Temperature dependence of the crystal and magnetic structures of $BiFeO_3$", *J. Phys. C: Solid State Phys.*, **13** (1980) 1931–1940.
23. P. Ravindran, R. Vidya, A. Kjekshus, H. Fjellvåg, O. Eriksson, "Theoretical investigation of magnetoelectric behavior in $BiFeO_3$", *Phys. Rev. B*, **74** (2006) 224412.
24. O.E. Gonzalez-Vazquez, J. Íñiguez, "Pressure-induced structural, electronic, and magnetic effects in $BiFeO_3$", *Phys. Rev. B*, **79** (2009) 064102.
25. J.F. Scott, R. Palai, A. Kumar, M.K. Singh, N.M. Murari, N.K. Karan, R.S. Katiyar, "New phase transitions in perovskite oxides: $BiFeO_3$, $SrSnO_3$, and $Pb(Fe_{2/3}W_{1/3})_{1/2}Ti_{1/2}O_3$", *J. Am. Cer. Soc.*, **91** (2008) 1762–1768.

26. A.G. Gavriliuk, V.V. Struzhkin, I.S. Lyubutin, S.G. Ovchinnikov, M.Y. Hu, P. Chow, "Another mechanism for the insulator-metal transition observed in Mott insulators", *Phys. Rev. B*, **77** (2008) 155112.
27. M. Guennou, P. Bouvier, G.S. Chen, B. Dkhil, R. Haumont, G. Garbarino, J. Kreisel, "Multiple high-pressure phase transitions in $BiFeO_3$", *Phys. Rev. B*, **84** (2011) 174107.
28. X.-X. Sun, Y.-L. Li, G.-H. Zhong, H.-P. Lü, Z. Zeng, "The structural, elastic and electronic properties of BiI_3: First-principles calculations", *Phys. B Condens. Matter.*, **407** (2012) 735–739.
29. R. Hill, "The elastic behaviour of a crystalline aggregate", *Proc. Phys. Soc. Sect. A.*, **65** (1952) 349–354.
30. C.J. Qi, Y.H. Jiang, R. Zhou, "First principles study the stability and mechanical properties of M_3B_2 (M = V, Nb and Ta) compounds", *Rare Met. Mater. Eng.*, **43** (2014) 2898–2902.
31. R. Ahmed, Fazal-e-Aleem, S.J. Hashemifar, H. Akbarzadeh, "First-principles study of the structural and electronic properties of III-phosphides", *Phys. B Condens. Matter*, **403** (2008) 1876–1881.
32. H. Hu, X. Wu, R. Wang, W. Li, Q. Liu, "Phase stability, mechanical properties and electronic structure of TiAl alloying with W, Mo, Sc and Yb: First-principles study", *J. Alloys Compd.*, **658** (2016) 689–696.
33. M. Chauhan, D.C. Gupta, "Phase stability, ductility, electronic, elastic and thermo-physical properties of TMNs (TM = V, Nb and Ta): An ab initio high pressure study", *Comput. Mater. Sci.*, **90** (2014) 182–195.
34. S.F. Pugh, "Relations between the elastic moduli and the plastic properties of polycrystalline pure metals", *Philos. Mag. Ser.*, **45** (1954) 823–843.
35. M. Chauhan, D.C. Gupta, "Electronic, mechanical, phase transition and thermo-physical properties of TiC, ZrC and HfC: High pressure computational study", *Diam. Relat. Mater.*, **40** (2013) 96–106.
36. S. Harsha Varthan, V. Nagarajan, R. Chandiramouli, "First-principles insights on mechanical and electronic properties of TiX (X = C, N) in β-Si_3N_4 based ceramics", *Process. Appl. Ceram.*, **10** (2016) 153–160.
37. A. Srivastava, R. Chandiramouli, "First-principles insights on electron transport in V_2O_5 nanostructures", *Mater. Sci. Eng. B.*, **201** (2015) 45–50.
38. R. Chandiramouli, V. Nagarajan, "Tuning band structure and electronic transport properties of ZrN nanotube – A first-principles investigation", *Spectrochimica Acta Part A*, **136** (2015) 1018–1026.
39. A. Srivastava, R. Chandiramouli, "Band structure and transport studies on impurity substituted InSe nanosheet - A first-principles investigation", *Superlattices Microstruct.*, **79** (2015) 135–147.
40. R. Chandiramouli, S. Sriram, V. Nagarajan, "Influence of oxygen, tellurium, and zinc substitution on CdSe nanoribbon: A First-principles investigation", *Synth. React. Inorganic, Met. Nano-Metal Chem.*, **45** (2015) 1780–1787.
41. R. Chandiramouli, "Exploring electronic transport properties of AlN nanoribbon molecular device – A first-principles investigation", *Solid State Sci.*, **39** (2015) 45–51.